



# A Technique for In-Situ Calibration of Semiconductor Strain Gauges Used in Hopkinson Bar Tests

Y. Miao<sup>1,2,3</sup> · X. Gou<sup>2,3</sup> · M.Z. Sheikh<sup>2,3</sup>

Received: 12 March 2018 / Accepted: 30 August 2018 / Published online: 7 September 2018  
© The Society for Experimental Mechanics, Inc 2018

## Abstract

The semiconductor strain gauges (SCSGs) are widely introduced in Hopkinson bar technique to detect weak strain signals of low-impedance materials, just for its high gauge factor. But, the measurement accuracy is negatively affected by the instability of SCSGs' specifications. A novel methodology is proposed to in-situ calibrate them and to interpret accurately the weak transmitted strain signals. And the dependence of the gauge resistance and factor on temperature and compressive/tensile loading conditions are calibrated with the stable electrical resistance strain gauges (ERSGs) as standard outputs. The results confirm that the properties present a high sensitivity to temperature, and even behave asymmetrically under tensile and compressive loadings. The experiments are carried out to verify the proposed in-situ calibration technique. Finally, the stress-strain curves of a shear thickening material are measured to demonstrate its reliability and detectability. This work will be useful to measure the dynamical mechanical properties of the soft and energy absorption materials like rubber and foams.

**Keywords** Hopkinson bar · Semiconductor strain gauge · Dynamic calibration · High strain rate

## Introductions

Engineering materials with low mechanical impedances have been widely used for specific applications, like foams extensively used in automotive and aerospace industries for their low specific mass and high specific strength [1], polymeric materials used in portable electronic industries for impact energy absorbing [2], and multifunctional cellulose composites for more extensive engineering applications due to their superior mechanical properties [3, 4]. Under these loading conditions, materials usually experience dynamic and impact

loadings. Therefore, it is necessary to know their mechanical behaviors under severe loading such as impact. The dynamic loading apparatus: split Hopkinson bar technique (short for SHPB), is widely used to measure the dynamic behavior of metallic materials under high strain rate loading [5–9]. Figure 1 shows the experimental setup of a typical SHPB, which mainly consists of a striker bar, incident bar, and a transmission bar. The specimen is sandwiched between the incident bar and the transmission bar.

During tests, the striker bar is projected towards the incident bar by a pressure in the gas gun chamber. Upon impact, a compressive wave is generated in the incident bar, which propagates towards the interface of the incident bar and specimen. At this interface, the incident pulse is partially reflected back into the incident bar and the rest is transmitted through the specimen into the transmission bar. The incident wave, reflected wave and transmitted wave are recorded by the strain gauges via Wheatstone bridge. Equation (1) is used to translate the voltage signals into the strain signals (more details are displayed in the following section). Finally, the one-dimension elastic wave theory is used to obtain the loading strain rate, strain and stress of the specimen from the recorded waves [6–10].

The low mechanical impedance of some materials is much lower than that of Hopkinson bar materials at least by one or

---

✉ M.Z. Sheikh  
sheikhzakir@mail.nwpu.edu.cn

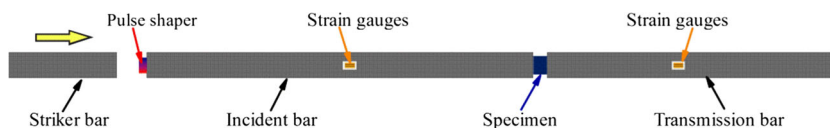
<sup>1</sup> State Key Laboratory for Strength and Vibration of Mechanical Structures, Department of Engineering Mechanics, School of Aerospace Engineering, Xi'an Jiaotong University, Xi'an 710049, Shaanxi, China

<sup>2</sup> Joint International Research Laboratory of Impact Dynamics and its Engineering Applications, School of Aeronautics, Northwestern Polytechnical University, Xi'an 710072, Shaanxi, China

<sup>3</sup> Shaanxi Key Laboratory of Impact Dynamics and its Engineering Application, School of Aeronautics, Northwestern Polytechnical University, Xi'an 710072, Shaanxi, China



**Fig. 1** Illustration of split Hopkinson bar apparatus



two orders of the magnitude. The stress signal in the transmission bar could also be so weak, even in the same order of magnitude of the system noise, that it is very difficult to detect the weak transmitted signals. In the past decades, however, great progress has been made. The preferred method is to reduce the impedance mismatch of the bar. Viscous-elastic Hopkinson bars were established with the aid of analytical solutions to wave dispersion in viscous-elastic bars [11–13]. Another method is to amplify the weak transmitted signals using appropriate techniques like aluminum tube to output the transmission bar signal [13], employing higher-sensitivity strain transducers such as the Quartz-crystal sensor [14], and incorporation of semiconductor strain gauges [15–17].

The electrical resistance strain gauges were firstly introduced in Hopkinson bar apparatus in 1964 [18] to record successfully the propagation of stress waves in long bars and became standard accessories for Hopkinson bar apparatus due to its accuracy and flexibility [19]. The semiconductor strain gauges are advantageous in recording the weak signals, just due to their high signal-to-noise ratios, and gauge factors even up to 150 (much higher than 2.1 of ERSG). Moreover, these are easy-to-use like ERSGs, and have been extensively employed in Hopkinson bar technique for testing low-impedance materials: polymer products [4, 15]; and bio-tissue [16]. But the instability of properties, which are sensitive to temperature and loading conditions, bring along some problems impairing the accurate strain measurement. The previous experimental investigations were based on the assumptions that specifications of SCSGs were stable, that is, constant electrical resistance and gauge factor, same as those of ERSGs. Unfortunately, this was not true in actual experiments because their electrical resistance was highly temperature-dependent and the gauge factors were hardly stable. They are also dependent upon both temperature and loading conditions, even present asymmetry under tension and compression loadings [20]. These instabilities must exert adverse influences on the measurement accuracy without a proper calibration. But, so far less published work is available for calibration of SCSGs.

In this paper, a novel methodology is proposed to calibrate the characteristics of SCSG used in Hopkinson bar technique. Based on the stable specifications of ERSGs, its output is selected as standard outputs to in-situ calibrate the specifications of SCSG. The resistance and gauge factor is calibrated in-situ under the loading of the Hopkinson bar technique. Verification experiments have been conducted to ensure the reliability of the methodology by using both ERSG and SCSG

simultaneously to pick up the transmission signals. Finally, experiments on a shear thickening material are conducted to demonstrate the feasibility of this in-situ calibration technique.

## Potential Problems

In order to display the probable problems of SCSG in detecting strain signals during the test, ERSG is additionally employed to pick up the standard output by cementing very closely to SCSG on the incident bar. When a compressive incident wave travels in the incident bar, it will be recorded by ERSG and SCSG, respectively. After the incident compression wave is reflected as tension wave at the interface of bar/specimen, it travels backward and is recorded by SCSG and ERSG again. The strain waves detected by SCSG and ERSG should be the same in amplitudes and configurations [6]. Therefore, considering the ERSG output as a standard reference, the SCSG responses can be analyzed under both compressive and tensile stress waves loading.

## Formula Deduction

The signal of strain gauges is recorded via a Wheatstone bridge, which is broadly used to measure strain in experimental mechanics. The specifically-designed bridge for this calibration work is shown as Fig. 2.

In Wheatstone bridge circuit,  $R_{adjust}$  is a slide rheostat with  $100\ \Omega$  to finely adjust the balance of circuit and  $E$  is the constant current.  $R_{SG}$  is designated with resistance  $1000 \pm 1\ \Omega$  and a gauge factor of  $2.1 \pm 1\%$  at room temperature (from BE1000-6AA, ZEMIC, China). The SCSG selected has nominal resistance  $1000 \pm 50\ \Omega$ , and a gauge factor of  $150 \pm 7.5$  at room temperature (HU-101 K from Saiying Electronic Technology Co. Ltd., China). The resistance  $R$  of ERSG

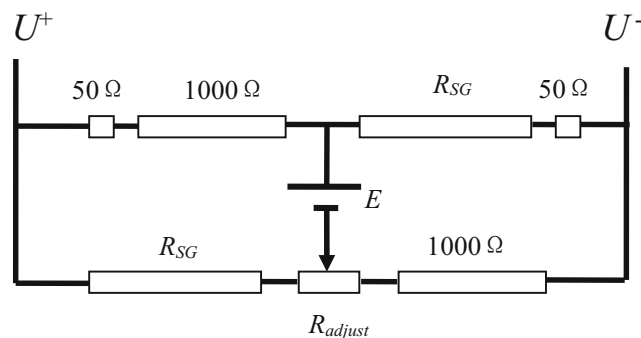


**Fig. 2** Wheatstone bridge circuit used in Hopkinson bar apparatus

changes with an increment  $\Delta R$  due to the load and  $\Delta U$  is output. Formerly, the following formula can be deduced for the strain-voltage output relation of the Wheatstone bridge circuit shown in Fig. 2:

$$\varepsilon = \frac{\Delta U}{E - \Delta U} \tag{1}$$

Supposing that SCSGs' initial resistance during experimenting (including the increment induced by temperature) be  $\hat{R}$ , and  $\Delta \hat{U}$  means the output voltage of SCSG Wheatstone bridge circuit, then the strain-voltage output relation for SCSG is given by:

$$\Delta \hat{U} = \frac{\hat{E} \cdot \hat{R} \cdot \hat{K} \varepsilon}{1100 + \hat{R}(1 + \hat{K} \varepsilon)} + \frac{\hat{E}(\hat{R} - 1000)}{1100 + \hat{R}(1 + \hat{K} \varepsilon)} \tag{2}$$

where the circumflex accent  $\wedge$  is used to differentiate the characteristic parameters of SCSG from those of the ERSG. The term,  $\frac{\hat{E}(\hat{R} - 1000)}{1100 + \hat{R}(1 + \hat{K} \varepsilon)}$  in equation (2), should be zero when the initial resistance  $\hat{R}$  equals its nominal value  $1000 \Omega$ . But this is nearly impossible due to its high sensitivity to temperature induced by ambient and the electric current of Wheatstone bridge. Thus, any temperature variation will result in some output of the signal, even without any stress loading. In the data processing, it is usually considered as an unnecessary deviation and neglected, so the strain signal can be deduced as given in equation (3):

$$\hat{\varepsilon} = \frac{1100 + \hat{R}}{\hat{K} \cdot \hat{R}} \cdot \frac{\Delta \hat{U}}{E - \Delta \hat{U}} \tag{3}$$

### Error Analysis

The specifications  $\hat{R}$  and  $\hat{K}$  are assumed to be  $1000 \Omega$ ,  $150$ , respectively. And the ambient temperature of SCSGs and ERSGs is  $24 \text{ }^\circ\text{C}$ . Figure 3 shows the incident wave and reflected wave in an experiment picked up from ERSGs and SCSGs, which are both cemented on the incident bar. There

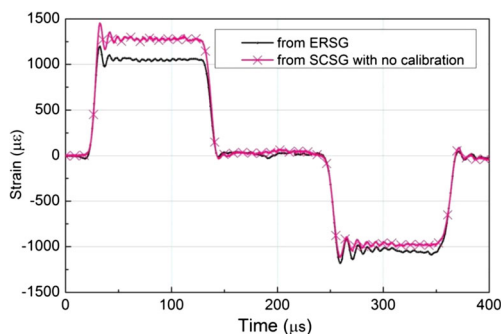


Fig. 3 Comparison of strain waves calculated from ERSG and SCSG without calibration

exists a distinct difference between the strain amplitudes of ERSG and SCSG.

It can be seen in Fig. 3 that without a proper calibration, SCSG flops in accurately interpreting the amplitudes of strain waves. The error of the ERSG reading could be up to  $21.33\%$  for the incident wave and  $-8.92\%$  for the reflected wave, respectively. It is also indicated that SCSG exhibits severe asymmetrical behavior under compressive and tensile load conditions. This is because the ambient influence and loading conditions result in significant deviation of the  $K$  and  $R$  values from the nominally specified. Lacking of the real resistance and gauge factor values goes against a reasonable interpretation of the SCSGs voltage data. To further quantitatively illustrate the influence, the resistance and factor are assigned a series of values around the nominal specifications to interpret the voltage data of SCSG. Figure 4a, b show the influences of different  $R$  and  $K$  values, respectively, where the highlighted lines are the interpretation of ERSG and will be used as a standard for comparison.

Figure 4 clearly demonstrates that the gauge factor and resistance influence significantly the gauge output, especially strain amplitudes. The peak strain values of the interpreted strain waves are selected to evaluate quantitatively the influence, as shown in Fig. 4c, which indicates that the strain amplitude is sensitive to the gauge factor: with the increasing  $K$ , the interpreted strain increases distinctly. Furthermore, it is not negligible for the effect of SCSG resistance as shown in Fig. 4b, d. And an error of up to about  $20\%$  can be estimated from Fig. 4c, d. Therefore, it is essential to determine the actual gauge factor and electrical resistance of SCSG during tests. And an in-situ calibration technique for properties of SCSG is critically required for the accurate measurement of strain.

### Specification Calibration

#### Calibration Procedures

In order to measure accurately the weak strain signal, a method is proposed to calibrate the SCSG in Hopkinson bar technique. ERSGs and SCSGs are cemented together on the incident bar and supposed to capture the same waves: the compressive incident wave and tensile reflected wave [4]. For one strain wave  $\varepsilon(t)$ , the response should be equivalent no matter it is recorded by ERSG or SCSG and interpreted by equations (1) and (3), respectively. Equation (4) is obtained by substituting equation (1) into equation (2).

$$f(\hat{K}, \hat{R}) = \hat{K} \cdot \hat{R} \cdot \frac{\Delta U}{E - \Delta U} - 2100 \cdot \frac{\Delta \hat{U}}{\hat{E} - \Delta \hat{U}} - (1000 - \hat{R}) = 0 \tag{4}$$

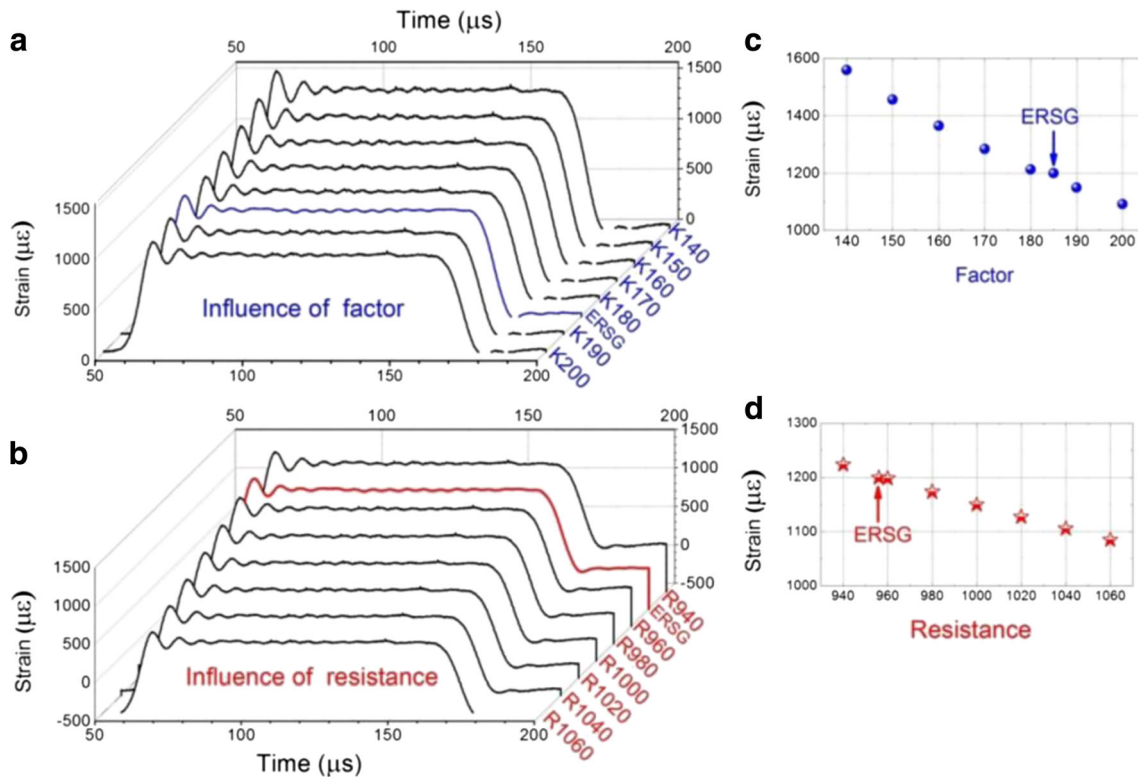


**Fig. 4** Influences of SCSG gauge factor and resistance, with (a):  $K$  increasing from 140 to 200, but  $R$  assumed to be stable at 1000  $\Omega$ ; (b):  $R$  increasing from 940 to 1060  $\Omega$ , but  $K$  is assumed to be stable at 150; (c)

and (d): the peak strain of the interpreted strain wave is introduced to analyses the influence of factor and resistance, respectively

There are only two unknown parameters  $\hat{K}$  and  $\hat{R}$  in equation (4). So, based on  $\Delta U$  and  $\Delta \hat{U}$  from the experimental data, the actual gauge factor  $\hat{K}$  and resistance  $\hat{R}$  can be solved by substituting voltage data detected by SCSGs and ERSGs into equation (4). With the experimental signals from Fig. 3, as an example, the characteristics of SCSGs in the incident bar are calibrated, and the curve calculated from SCSG with calibration is shown in Fig. 5 together with the curve calculated from ERSGs. The calibrated  $\hat{K}$  and  $\hat{R}$  values under compressive (the incident wave) and tensile (the reflected wave) loadings are shown in Table 1 in the row for the temperature of 24  $^{\circ}C$ .

It is evident in Fig. 5 that there are no obvious differences between the strains from the ERSGs and the calibrated SCSGs. Thus, the feasibility and reliability of the calibration methodology implemented in this work are established by the good agreement in terms of both the strain amplitudes and the fluctuating characteristics.

## Temperature Effects

Different temperature experiments are designed to investigate the dependence of SCSGs at a lower temperature (9 $^{\circ}C$ ), room temperature (24 $^{\circ}C$ ), and an elevated temperature (40 $^{\circ}C$ ), respectively. The lower temperature is realized by spraying the cooled air mixed with the vaporized liquid nitrogen on SCSGs

[21] and the elevated temperature is achieved by heating the ring-type furnace which surrounds the SCSGs cemented on the calibrated Hopkinson bar. An instrument equipped with a thermocouple is used to in-situ monitor the SCSGs' temperature [10]. The desired temperature is achieved and kept constant at least for five minutes before dynamic loading. The experiments at each temperature are repeated at least four times to ensure the experimental reliability.

The calibrated parameters in Table 1 indicate that the temperature influences noticeably the resistance of SCSG. The resistance decreases with temperature increase, while they are very close to each other under both compressive and tensile loading. Thus, it is concluded that SCSG resistance is consistent

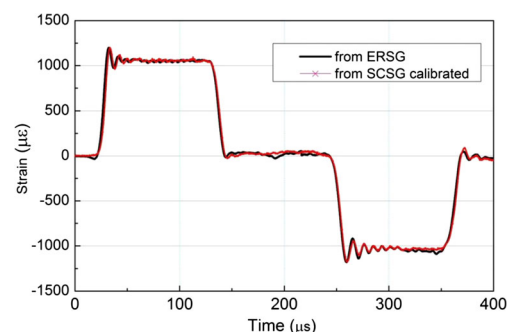


**Fig. 5** Comparison of strain waves calculated from ERSG and calibrated SCSG

**Table 1** Gauge resistances and factors of SCSG calibrated

	Compressive loading		Tensile loading	
	Resistance(Ohm)	Factor	Resistance(Ohm)	Factor
9°C	1052.14	187.24	1052.09	146.77
24 °C	999.38	190.16	998.39	142.39
40°C	956.74	181.65	957.01	142.88
Specification*	1000 ± 5%	150 ± 5%	1000 ± 5%	150 ± 5%

Specifications\* are offered from the manufactory company, with the temperature coefficient of resistance <0.40%, the temperature coefficient of the gauge factor <0.30% and the reference temperature 25°C

and show no sensitivity to loading conditions. But, the gauge factor drops sharply from more than 180 under the compressive loading to less than 150 under the tensile loading at each investigated temperature. Severe asymmetrical behaviors occur under compressive and tensile loading. This coincides with the fact that a gauge factor under compression is higher than that under tension for SCSGs [22]. So, this asymmetrical property accounts for the fact that the interpreted reflected wave is lower than the incident wave as shown in Fig. 3.

## In-Situ Calibrations

### In-Situ Calibration Methodology

The above-mentioned calibration method in section 3.1 is introduced directly in Hopkinson bar experiments while testing dynamic behaviors of low-impedance materials. The SCSGs are cemented on the transmission bar for detecting weak transmission strain wave. The in-situ calibration methodology is as follows: in the experiment, the SCSGs of both the incident and transmitted bar are equivalently affected by the same ambient temperature and loading conditions, and they should have the same resistances and gauge factors. Based on the calibration procedure in section 3, actual resistances and gauge factors of SCSG on the incident bar can be obtained, and then they are extended to the SCSGs of the transmission bar since they are under the same ambient conditions. Therefore, the SCSGs output can be interpreted accurately. Consequently, the weak transmission strain wave during low-impedance materials testing can be measured via SCSG with the same accuracy level as that of ERSG.

**Table 2** Mechanic parameters and dimension of bar and specimen

	Striker bar	Incident/Transmission bar	Specimen
Diameter (mm)	15	15	7
Length/Thickness (mm)	200	2000	7
Elastic Modulus (MPa)	71,000	71,000	NA

To verify the in-situ calibration technique, an experiment is conducted on the calibrated Hopkinson bar apparatus. A couple of ERSGs and SCSGs are cemented both on the incident and transmission bar. Thus, the two couples of ERSGs, as the traditional output of the Hopkinson bar test, would interpret the strain signals to strain rate, strain, and stress to generate the stress-strain curve for reference. The SCSGs' output can be interpreted based on the aforementioned calibration methodology, through which the stress-strain curve is obtained too. The mechanical parameters and the dimensions of the bar and specimen used in tests are illustrated in Table 2. The specimen was a polymeric material.

In the experiment, the incident and reflected waves are recorded by both ERSGs and SCSGs on the incident and transmission bars. Like the traditional procedure of the Hopkinson bar technique, the stress-strain curve can be calculated based on the traditional ERSGs' signals of the incident and transmission bars, and shown in Fig. 6. Using the calibration technique, SCSGs' signals of the incident bar and transmission bar are in-situ calibrated to obtain the actual resistance and gauge factor, then the stress-strain curve is obtained, and presented in Fig. 6 together. It is indicated that the two curves are in good agreement, which verifies that the reliability of the methodology based on the in-situ calibration technique can achieve nearly the same level of accuracy as the traditional ERSGs.

### Experiments of the Low-Impedance Material

A shear thickening material is selected to check the detectivity of the in-situ calibrated Hopkinson bar technique. The details of the apparatus and specimen are the same as those illustrated in Table 2, except the incorporation of a longer striker bar with

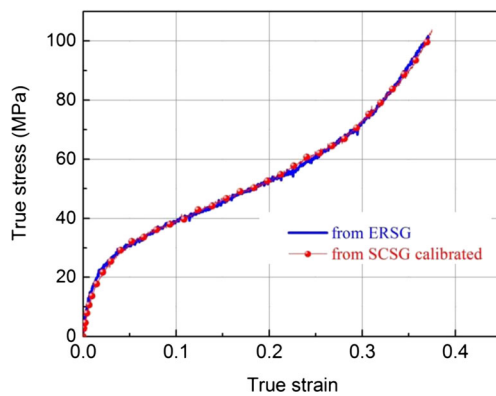


**Fig. 6** Curves comparison from in-situ calibrated SCSG and a traditional ERS

a length of 0.70 m. The pulse shaping technique is introduced to trim the incident wave to attain the desired loading characteristics with more rapid stress equilibrium and constant strain rate [9, 10]. A typical stress-strain curve is obtained and shown in Fig. 7, along with the corresponding true strain rate. A series of experiments are also conducted to study the strain rate effect for this material, and the curves are shown together in Fig. 8. With the strain rate increasing from  $1300 \text{ s}^{-1}$  to  $4100 \text{ s}^{-1}$ , the stress increases sharply by around 11.4 times ( $(31.8 \text{ MPa})/(2.78 \text{ MPa})$ ) at a true strain of 0.3). This demonstrates that the high rate-dependence of the mechanical response of this material. It can be demonstrated in Figs. 7 and 8 that the stress can be detected even when it is much lower than 1 MPa below the true strain of 0.10. The measurement detectivity can be further improved by using transmission bars made of polymeric materials [15].

## Conclusions

An in-situ calibration method is proposed for calibrating the specifications of SCSGs, which is used in the Hopkinson pressure bar to detect the weak strain signal while testing low-impedance materials. The resistance and gauge factor of SCSGs used in the experimental set-up are in-situ calibrated

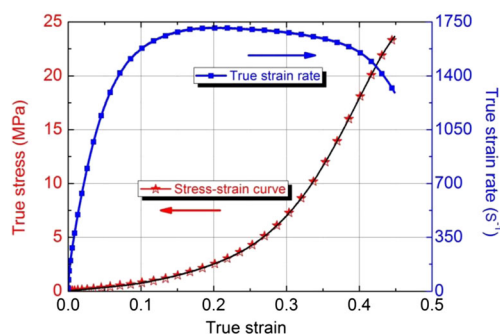


**Fig. 7** Stress-strain curve of a shear thickening material under strain rate  $2300 \text{ s}^{-1}$  by using this calibration

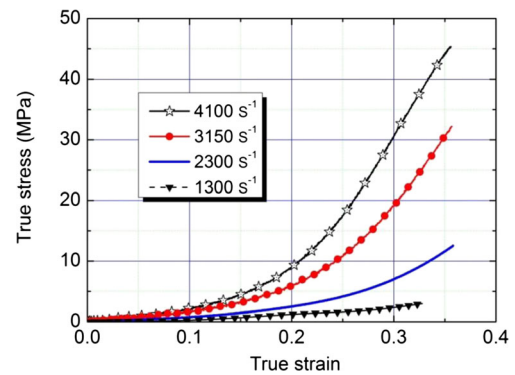


**Fig. 8** Stress-strain curves of the shear thickening material under different strain rates

by taking the output of ERS as standard. Experiments are also conducted with calibrated set-ups for investigating the influence of temperature and different loading conditions, and the results indicate that the resistance of SCSG is sensitive to temperature, and the gauge factor presents high asymmetrical behavior under compressive and tensile loading conditions. Finally, the methodology is proposed to in-situ calibrate the nominal properties of SCSGs and simultaneously test low-impedance materials using a Hopkinson bar technique. The experimental results on the shear thickening material demonstrate that the detectivity can be as low as 1 MPa for aluminum Hopkinson bar apparatus, which could be useful to accurately measure the dynamical mechanical properties of the rubber-like materials and foam-like energy absorption materials.

**Acknowledgments** We would like to thank the financial support by National Natural Science Foundation of China and Natural Science Foundation of Shaanxi Province (#2018JQ1040), and Dr. Hong-Yuan Liu from the University of Sydney for the helpful discussion.

## References

- Hou B, Ono A, Abdennadher S, Pattofatto S, Li YL, Zhao H (2011) Impact behavior of honeycombs under combined shear-compression. Part I: experiments. *Int J Solids Stru* 48(5):687–697
- Song B, Chen W, Jiang X (2005) Split Hopkinson pressure bar experiments on polymeric foams. *Int J Vehi Desi* 37(2/3):185–198
- Meng Q, Li B, Li T, Feng XQ (2017) A multiscale crack-bridging model of cellulose nanopaper. *J Mech Phys Solids* 103:22–39
- Meng Q, Li B, Li T, Feng XQ (2018) Effects of nanofiber orientations on the fracture toughness of cellulose nanopaper. *Eng Fract Mech* 194:350–361
- Hopkinson B (1914) A method of measuring the pressure in the deformation of high explosives or by the impact of bullets. *Phil Trans Roy Soc London A* 213:437–452
- Kolsky H (1949) An investigation of the mechanical properties of materials at very high rates of loading. *Proc. Roy. Soc. London B* 62:676–700
- Miao YG, Li YL, Liu HY et al (2016) Determination of dynamic elastic modulus of polymeric materials using vertical split Hopkinson pressure bar. *Int J Mech Sci* 108–109:188–196

8. Wang S, Flores-Johnson EA, Shen L (2017) A technique for the elimination of stress waves overlapping in the split Hopkinson pressure bar. *Expe Tech* 41:345–355
9. Tan X, Guo W, Gao X, Liu K, Wang J, Zhou P (2017) A new technique for conducting split Hopkinson tensile bar at elevated temperatures. *Exp Tech* 41:191–201
10. Miao YG (2018) On loading ceramic-like materials using split Hopkinson pressure bar. *Acta Mech* 229:3437–3452
11. Wang L, Labibes K, Azari Z, Pluvinage G (1994) Generalization of split Hopkinson bar technique to use viscoelastic bars. *Int J Imp Eng* 15:669–686
12. Zhao H, Gary G (1995) A three dimensional analytical solution of the longitudinal wave propagation in an infinite linear viscoelastic cylindrical bar: application to experimental techniques. *J Mech Phys Solids* 43(8):1335–1348
13. Chen W, Zhang B, Forrestal MJ (1999) A split Hopkinson bar technique for low-impedance materials. *Exp Mech* 39(2):81–85
14. Chen W, Lu F, Zhou B (2000) A quartz-crystal-embedded split Hopkinson pressure bar for soft materials. *Exp Mech* 40(1):1–6
15. Miao, Y.G. Li, Y.L. Deng, Q. Tang, Z.B. Hu, H.T. Suo, T. (2015) Investigation on experimental method of low-impedance materials using modified Hopkinson pressure bar. *J Beijing InstTech* 24(2): 269–276
16. Pervin F, Chen W, Weerasooriya T (2011) Dynamic compressive response of bovine liver tissues. *J Mech Beha Biomech Mate* 4:76–84
17. Zhang J, Yoganandan N, Pintar FA, Guan Y, Shender B, Paskoff G, Laud P (2011) Effects of tissue preservation temperature on high strain rate material properties of brain. *J Biomech* 44:391–396
18. Lindholm US (1964) Some experiments with split Hopkinson pressure bar. *J Mech Phys Solids* 12(3):317–335
19. Miao YG, Du B, Sheikh MZ (2018) On measuring the dynamic elastic modulus for metallic materials using stress wave loading techniques. *Arch Appl Mech*. <https://doi.org/10.1007/s00419-018-1422-6>
20. Lüder E (1986) Polycrystalline silicon-based sensors. *Sensors Actuators* 10:9–23
21. Suo T, Li YL, Zhao F, Fan XL, Guo WG (2013) Compressive behavior and rate-controlling mechanisms of ultrafine grained copper over wide temperature and strain rate range. *Mech Mat* 61:1–10
22. Window AL, Holister GS (1982) Strain gauges technology. Applied Science Publishers